JCSE The Journal of Corrosion Science and Engineering

Century 21st Corrosion Science

Volume 6 Paper H029

Electrochemical behavior of Fe-28Al-2C after high temperature hydrogen treatment

T. Laha[a], R. Balasubramaniam[a,*], A. Tewari[a], M.N. Mungole[a] and R.G. Baligidad[b]

[a] Department of Materials and Metallurgical Engineering
Indian Institute of Technology, Kanpur 208 016, INDIA.

[b] Defence Metallurgical Research Laboratory, Hyderabad 500 058, INDIA.

Abstract

The effect of high temperature heat treatment on the electrochemical behavior of a carbon-alloyed iron aluminide of composition Fe-16.2Al-0.54C (in wt %) was studied by potentiodynamic polarization studies. The electrochemical behavior of the as-received alloy was characterized in sulfuric acid of different normalities. Well-polished samples were exposed to hydrogen at 1 atmospheric pressure at 700°C and 900°C for different times. The effect of high temperature hydrogen treatment on the electrochemical behavior of the alloy was addressed. The high temperature treatment did not affect the secondary anodic peak observed in the polarization experiments. The increase in passive range and passive current densities of the hydrogen treated samples, with increasing treatment temperature and time, was attributed to surface compositional changes, which was confirmed by microhardness studies.

KEYWORDS: Iron aluminides, hydrogen treatment, electrochemical behaviour, microhardness

* Author for correspondence

This paper was presented at the Conference "Corrosion Science in the 21st Century" held at UMIST in July 2003.

1. Introduction

There is an increasing interest in the development of high temperature materials based on intermetallic phases. Intermetallic alloys based on iron aluminides, centered around the stoichiometric compositions Fe_3Al and FeAl, are being considered for high temperature structural applications. Specific advantages of iron aluminides include excellent sulphidation resistance, very good oxidation resistance, lower density (5400-6700 kg/m^3) which is 30% lower than that of the commercially available high temperature materials, good wear resistance, good cavitation erosion resistance and potential lower cost [1]. Although these alloys exhibit poor room temperature ductility and low fracture toughness, significant improvements have been achieved by alloying additions and process control [1]. The available literature generally addresses iron aluminide compositions with very low (<0.01 wt%) carbon contents because it was reported that carbon reduced ductility [2]. Recently, Baligdad *et al* reported that addition of carbon in the range of 0.14 to 1.1 wt % significantly increased the strength and hardness of iron aluminides, which was attributed to solid solution strengthening by interstitial carbon in the matrix, to the precipitation of perovskite-based $Fe_3AlC_{0.5}$ phase and the formation of a duplex Fe_3Al-$Fe_3AlC_{0.5}$ structure [3-5]. The moderate ductilities exhibited by these alloys have been related to irreversible trapping of hydrogen at bulky carbide-matrix interfaces [6]. An added advantage in these iron aluminides of high carbon content is their excellent machinability, which is due to the presence of uniform carbide precipitates that facilitate the formation of small, uniform-sized chips during machining [4]. One of the key factors in increasing the maximum use temperature is enhanced resistance to high temperature atmospheres. The Fe-Al alloys with higher aluminum and carbon contents are more resistant to oxidation and decarburization [7]. A better oxidation resistance appears to lead to resistance to decarburization in these alloys [8]. The hot corrosion resistance of the carbon-alloyed iron aluminides was superior compared to the base iron aluminide (i.e. without any carbon addition), which has been attributed to the presence of carbides that hinder the diffusion of damaging species down grain boundaries [9,10].

It was reported recently that the experimental potentiodynamic polarization curves of several carbon-alloyed iron aluminide alloys (Fe-15.6Al-0.05C, Fe-15.6 Al-0.14C, Fe-15.6Al-0.5C-Fe-15.6Al-1C, in wt %) exhibited a typical secondary anodic peak[11]. Frangini *et al.* [12] did not, however, report the existence of secondary anodic peak in a hot rolled iron aluminide alloy containing 24.4 wt % Al. The appearance of the secondary anodic peak in acid solution has been

proposed to be due to the reoxidation of absorbed hydrogen atoms on the surface [13]. It was, therefore, decided to understand this phenomenon by controlled exposure of a carbon-alloyed iron aluminide to hydrogen at high temperature for several different times. The aim of the present study is to characterize the electrochemical behavior of a carbon-alloyed iron aluminide after high temperature hydrogen treatment.

2. Experimental

An iron aluminide ingot of composition Fe-16.2Al-0.54C (in wt %), which corresponds to Fe-28.1Al-2.1C in at %, was prepared by air induction melting and chill cast into a cast iron mould. Commercial purity aluminum and mild steel scrap were used as raw materials. Grinding was used to clean the surface of the iron charge. After melting, the slag product was skimmed off. Aluminium pieces were then added to the molten iron bath. The melt was held at 1620^{o} C for a very short time (2 minutes) to prevent aluminum losses and then normalized to room temperature. The ingot was then tested for its soundness by radiography. The ingot (55 mm diameter, 360 mm long) was machined to 50 mm diameter. They were refined in an electro-slag remelting (ESR) furnace of 350 kVA capacity. A commercial prefused flux based on CaF_2 was used. The flux was preheated and held at 850^{o}C for 2 hours before use in order to remove moisture. The iron aluminide electrode was remelted under this flux cover and cast into 76 mm ingot in a water cooled steel mould. At the end of the process, the power supply was gradually reduced to impose a condition of hot topping. The ESR ingots were also radiographed to check their soundness. The ingots were then forged to a reduction ratio of 70% and subsequently hot rolled down to strips of 3 mm thickness. The alloy exhibited recrystallized grains after thermomechanical processing. Rectangular specimens (of approximate size 8mm×5mm×3mm) were cut from the alloy strips using a diamond cutter (ISOMET, Buehler). All the surfaces of the specimens were mechanically polished in fine cloth using 0.5μ alumina powder and then degreased using acetone before each experiment.

The apparatus for hydrogen attack studies consisted of a tube furnace, a hydrogen gas cylinder, a argon gas cylinder, a gas pressure controller and a gas train. A vertical tube furnace of 150 mm length was employed. Temperature profiling of the furnace showed that a constant temperature zone of about 25 to 30 mm was obtained in the central region of the furnace. The temperature of the furnace was controlled within ±2K and measured by a Pt/Pt-10%Rh thermocouple. A mullite tube (45 mm inner diameter and 460 mm length) acted as the reaction

chamber. The mullite tube was fitted with silicone rubber stopper at the top to provide airtight fitting cover. The gas inlet tube and outlet tubes were inserted through the top of the reaction chamber through the silicone rubber stopper. All these tubes were glass fitted with rubber tubing and sealed with sealant. Teflon tapes were tightly wound on the locations where the glass tubes were fit with the rubber tubes. The specimen was placed inside a quartz crucible with three holes at the bottom to allow easy passage of gas. This crucible was then hung from the top of the furnace using a platinum wire into the reaction zone of the chamber. The experiments were carried out isothermally. Once the furnace attained the test temperature, sufficient time (15 to 20 minutes) was allowed for temperature to stabilize. The furnace was then first flooded with argon gas for 10 minutes to remove all entrapped air and then again hydrogen gas was purged in the reaction chamber to remove the argon gas and to maintain the reaction environment condition inside the furnace before introduction of the sample. A gas train was utilized to monitor the flow rates of the gas and purify it from probable impurities present. Pure gas was passed through a bubbler and capillary flow meter. The gas was then passed through an Ascarite (sodium hydroxide coated silica) column to remove carbon dioxide. It was then passed through anhydrous calcium chloride and Drierite ($CaSO_4$) columns successively before introduction into the reaction chamber. Drierite possesses low equilibrium residual water vapor pressure and therefore, it was used after the anhydrous calcium chloride column in the gas train for efficient removal of moisture. The outlet gas was passed out of the furnace through a bubbler to ensure that the flow of gas was being maintained through the system.

Hydrogen treatment was performed for five different conditions changing the treatment temperature and time (at 700^{o}C for 10 h and 48 h, and at 900^{o}C for 144 h, 336 h, 720 h) at one atmospheric hydrogen pressure. The experiment at 900^{o}C for 144h was repeated for duplicate testing. The samples, after hydrogen treatment, were slightly polished to remove a thin oxide layer that had formed on high temperature exposure and utilized for electrochemical studies.

Electrochemical polarization studies were conducted using a Perkin Elmer potentiostat (Model 263A) and a flat cell. A silver/silver chloride (SSC) electrode in saturated KCl was used as the reference electrode and the counter electrode was a platinum grid. All the potentials reported in the paper are with respect to SSC electrode (+197 mV vs standard hydrogen electrode). Two sets of experiments were conducted. In the first set, the as-received sample, that had not been treated with hydrogen, was tested at different normalities of H_2SO_4 from 0.1 N to 1.0 N to study the effect of acid concentration. In the second set, experiments were carried out in a solution of 0.5 N

sulfuric acid on the samples after exposure to hydrogen. The potentiodynamic polarization experiments were carried out in the potential range of –700 mV to +1600 mV for all the samples. The experiments were started immediately after immersion of the alloy in the electrolyte. All the polarization experiments were carried out at a scan rate of 0.5 mV/s.

3. Results and discussion

Microstructures

A typical microstructure of the as-received material is presented in Figure 1. Two different morphologies of second phase carbide particles were observed: bulky and needle-shaped. The microstructural aspects after the treatments have been discussed in details elsewhere [14].

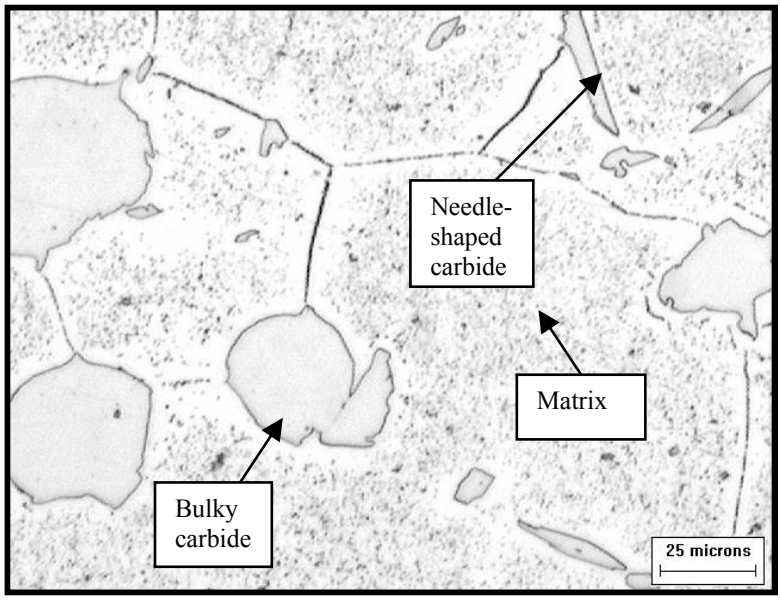

Figure 1. Microstructure of the as-received aluminide showing grain boundaries, bulky carbides and needle-shaped carbides.

The needle shaped carbides dissolved in the matrix fairly early. The bulky carbides were degraded along the {111} and {110} crystallographic directions, which has been explained by considering its crystal structure The interfaces between bulky carbides and matrix were affected by the heat treatment, the degradation increasing with increasing time and temperature.

Effect of pH

Figure 2 shows the potentiodynamic polarization behavior of the alloy at different normalities of H_2SO_4. The corrosion rate (i_{corr}) and Tafel slopes (β_c and β_a) at different normalities of H_2SO_4 solution were determined from the potentiodynamic polarization curves and are tabulated in Table 1.

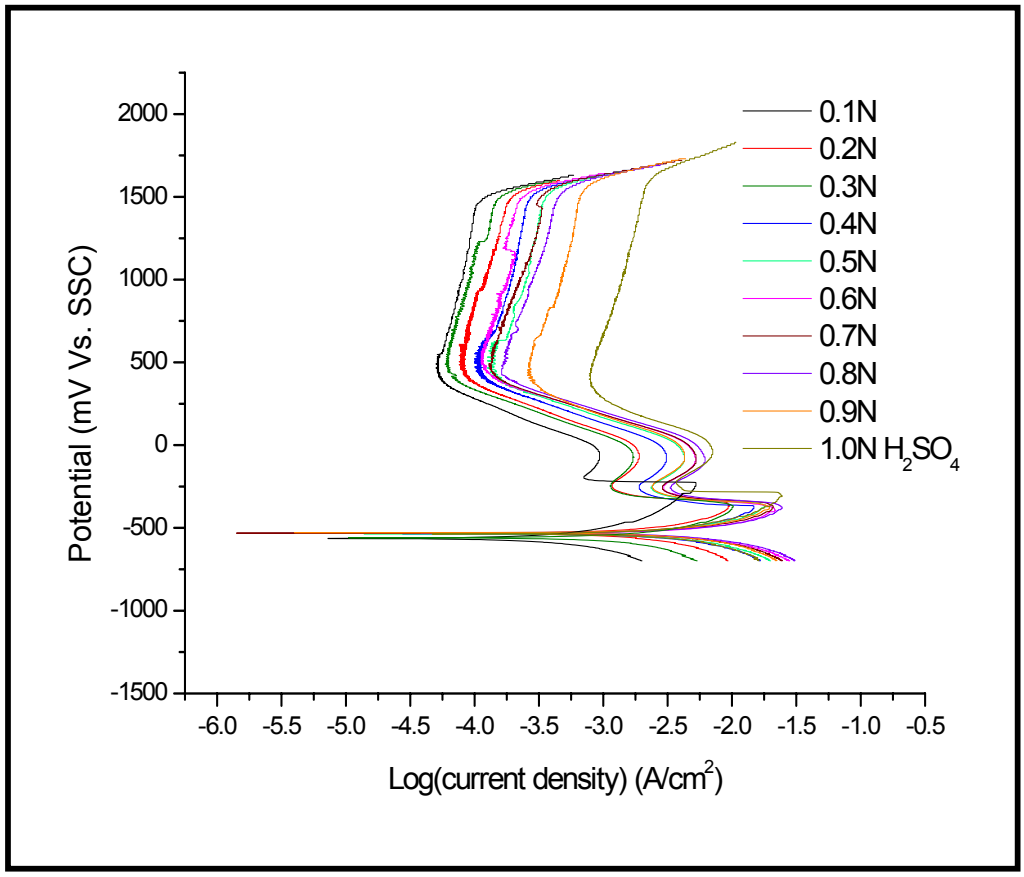

Figure 2. Potentiodynamic polarization behavior of as-received aluminide in sulfuric acid of different normalities.

Table 1.Values of β_a, β_c and i_{corr} obtained from the potentiodynamic polarization curves of as-received aluminide in sulfuric acid of different normalities

Normality of H_2SO_4 (N)	β_c (V/decade)	β_a (V/decade)	i_{corr} (mA/cm^2)
0.1	-0.254	0.182	0.41
0.2	-0.245	0.190	2.24
0.3	-0.316	0.188	1.90
0.4	-0.242	0.187	3.42
0.5	-0.247	0.190	4.13
0.6	-0.248	0.174	5.12
0.7	-0.252	0.190	5.29
0.8	-0.251	0.189	6.17
0.9	-0.262	0.160	6.31
1.0	-0.264	0.196	6.31

The β_c and β_a values were almost similar in different normalities of H_2SO_4. The β_c values varied in the range of –0.242 to -0.264 V/decade, whereas the β_a values were in the range of 0.174 to 0.196 V/decade. However, the corrosion rate (i_{corr}) increased continuously and systematically (from 0.41 $mAcm^{-2}$ for 0.1 N to 6.31 $mAcm^{-2}$ for 1.0 N) with increasing normality of the H_2SO_4. The concentration of H^+ ion increases with increasing normality and the rate of cathodic reaction (hydrogen evolution reaction) also increases with higher H^+ ion concentration. One reason for the observed increase in the anodic reaction rate (i.e. corrosion rate) was, therefore, the higher concentration of H^+ available with increasing normalities.

The potentiodynamic polarization curves, obtained as a function of solution normality (Figure 2) exhibited active-passive behavior. The values of zero current potential (ZCP), complete passivation potential (E_{cp}), transpassive potential (E_{tp}) and passive current density (i_{pass}) were obtained from the potentiodynamic polarization curves (Figure 2) and these are summarized in Table 2.

Table 2. Passivation parameters obtained from the potentiodynamic polarization curves of as-received aluminide in sulfuric acid of different normalities

H_2SO_4	ZCP	E_{pp1}	E_{pp2}	E_{cp}	E_b	E_b-E_{cp}	i_{crit1}	i_{crit2}	i_{pass}	$i_{0_{H^+/H_2}}$
N	mV						mA/cm^2			
0.1 N	-554	-238	-65.6	439	1420	981	5.25	0.98	0.051	0.09 X 10^{-2}
0.2 N	-543	-362	-63.7	493	1460	967	9.55	1.86	0.080	1.61 X 10^{-2}
0.3 N	-560	-357	-56.7	478	1430	952	7.94	1.35	0.060	3.31 X 10^{-2}
0.4 N	-544	-364	-59.3	497	1470	973	14.79	3.09	0.100	2.50 X 10^{-2}
0.5 N	-535	-370	-65.6	501	1480	979	18.20	4.36	0.132	2.95 X 10^{-2}
0.6 N	-535	-385	-78.9	517	1470	953	21.88	5.37	0.110	4.68 X 10^{-2}
0.7 N	-544	-393	-66.5	482	1490	1008	21.38	5.25	0.134	4.68 X 10^{-2}
0.8 N	-522	-385	-92.3	437	1490	1053	22.51	6.03	0.162	5.50 X 10^{-2}
0.9 N	-537	-375	-59.3	439	1520	1081	19.50	4.47	0.250	5.62 X 10^{-2}
1.0 N	-546	-320	-45.4	431	1550	1119	22.13	7.08	0.776	6.16 X 10^{-2}

The ZCP, E_{cp} and E_{tp} were almost similar in different normality solutions. However, i_{pass} generally increased with increasing normality of H_2SO_4. The value of i_{pass} in case of 0.2 N H_2SO_4 was slightly more than that in case of 0.3 N H_2SO_4, the reason for which could not be understood. All experiments were duplicated and the results were highly reproducible. The increasing passive current density with decreasing pH has been recognized [15] and the results of the present study are in conformity with literature. In order to obtain some insights on the dominant reduction reaction in the cathodic region of the polarization diagram, the ZCP was compared with the reversible potential for hydrogen evolution reaction. Table 1 indicates that the ZCP values of the alloy were in the range between -522 to –566 mV vs SSC. The equilibrium reversible potential for the hydrogen evolution reaction was calculated by Nernst equation to be slightly noble compared to the observed ZCP values. Therefore, it can be concluded that hydrogen evolution was the dominant cathodic reaction. Analysis of the transpassive region was also similarly undertaken. The transpassive potential (E_{tp}) for the samples were compared with the equilibrium reversible potential for the oxygen evolution reaction. As the estimated reversible potentials were moderately active

compared to the transpassive potential (E_{tp}), the transpassive region was concluded to be due to oxygen evolution.

The polarization diagrams (Fig. 2) showed an extra anodic peak in addition to the first peak, in conformity with literature [11]. The first anodic peak was observed in the range between –238 mV to –393 mV for different normalities of H_2SO_4 solution. A secondary anodic peak was observed in the range of –45 mV to –92 mV before reaching the broad passive zone of constant passive current density. It is important to note that the secondary anodic peak was observed for all the normalities of the solution used. The primary passivation potentials (E_{pp}) and critical current densities (i_{crit}) were calculated for both the peaks and tabulated in Table 2. The subscript 1 denotes the active peak and the subscript 2 denotes the nobler peak (i.e. the secondary anodic peak). The E_{pp1} and E_{pp2} did not vary significantly in different normality solutions. Although the values of i_{crit1} exhibited an increase with normalities for some cases (for example, when 0.4 N H_2SO_4 was used as the electrolyte instead of 0.3 N H_2SO_4), a general trend of increasing i_{crit1} with increasing normality was not observed. On the other hand, the i_{crit2} values increased with increasing normality. As can be noticed in the polarization diagrams (Fig. 2), a larger amount of hydrogen was reduced (indicated by larger cathodic current densities at any fixed potential active to ZCP) when the specimen was first polarized in the cathodic region (during the potentiodynamic polarization experimental scan) with increasing H^+ concentration in electrolyte. Therefore, the increasing i_{crit2} for the second anodic peak can be explained by the larger amount of hydrogen available for oxidation in solutions of higher nomalities.

The exchange current density for the hydrogen evolution reaction ($i_{0_{H^+/H_2}}$) was also stimated by extending the cathodic Tafel slope and intersecting it with the parallel line to log (i) axis at the equilibrium reversible potential for the reaction. It is evident from Table 2 that the exchange current densities increased with increasing normality of H_2SO_4. Therefore, this could be another plausible reason for the observed increase in corrosion rate with increasing H^+ concentration, especially since the Tafel β_c slope was not affected by normalities. The estimated exchange current densities were comparable to those obtained on other carbon-alloyed iron aluminides [11]. Moreover, the exchange current densities were an order of magnitude higher than that on iron (2.0×10^{-3} mA/cm^2 in 0.5N H_2SO_4) [11] and by several orders of magnitude higher than that on Al (7.9×10^{-7} mA/cm^2 in 0.5N H_2SO_4) [11]. The enhanced hydrogen reaction kinetics in carbon alloyed iron aluminides must be related to the presence of carbides in the microstructure.

This is indirectly indicated by higher exchange current densities reported for an Fe-15.6Al-1.0C alloy (50.1 x 10^{-2} mA/cm^2 in 0.5N H_2SO_4 [11]).

Effect of hydrogen treatment

The normality of the electrolyte chosen for conducting the potentiodynamic polarization experiments on the hydrogen treated samples was 0.5 N H_2SO_4. The potentiodynamic polarization curves are shown in Figure 3. The β_c, β_a and i_{corr} values, determined from these results, were almost similar for all the samples (Table 3). Therefore, high temperature hydrogen treatment did not have any significant effect on corrosion rate, thereby indicating that corrosion rate is primarily determined by the normality of the electrolyte.

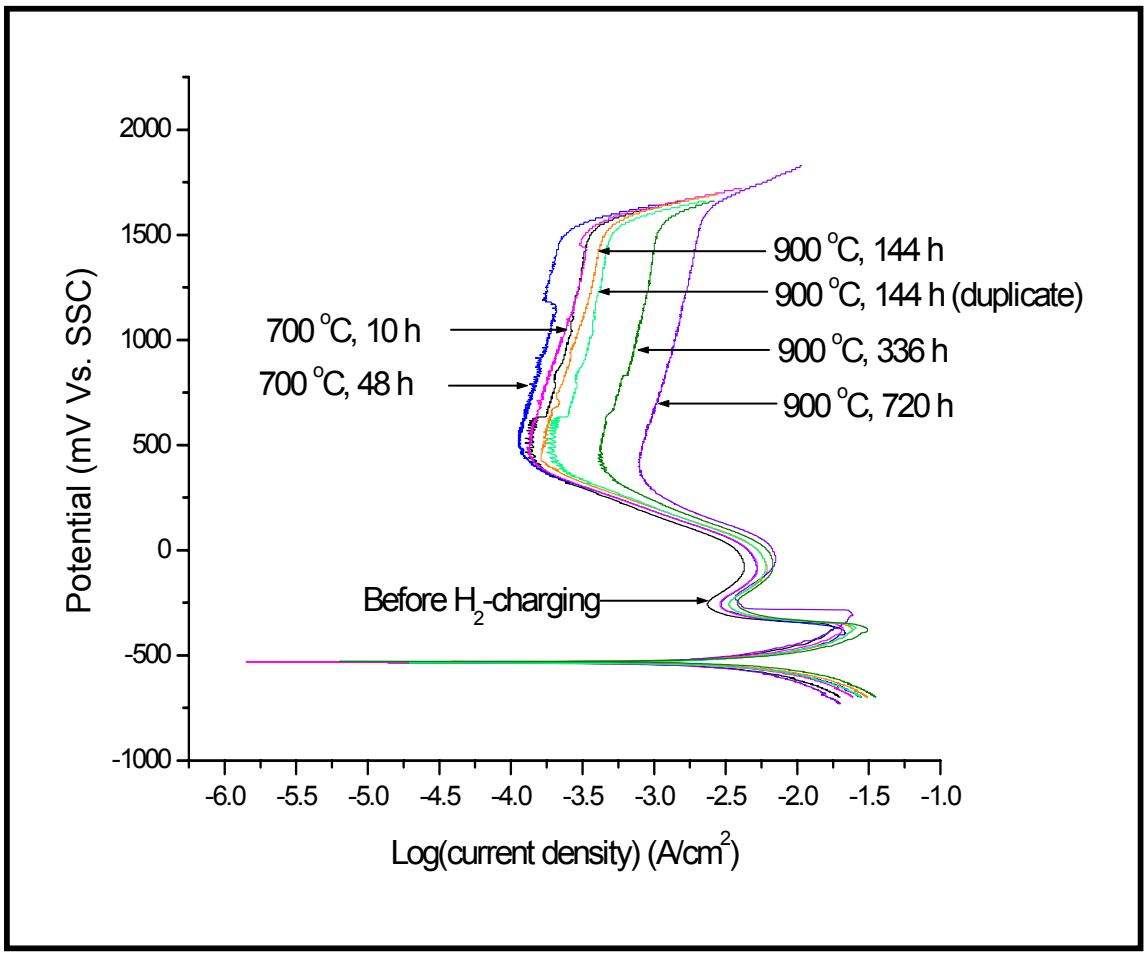

Figure 3. Potentiodynamic polarization behavior of hydrogen treated Fe-16.2Al-0.54C (wt%) samples in 0.5 N H_2SO_4 solution

Table 3 Values of β_a, β_c and i_{corr} obtained from the potentiodynamic polarization curves of the hydrogen treated samples in 0.5 N H_2SO_4 solution.

Sample		β_c	β_a	i_{corr}
Temp. (^oC)	Time (h)	(V/decade)	(V/decade)	(mA/cm^2)
Without treatment		-0.247	0.190	4.13
700	10	-0.248	0.172	5.15
700	48	-0.250	0.187	5.25
900	144	-0.249	0.190	5.99
900	144	-0.246	0.184	5.76
900	336	-0.251	0.189	6.21
900	720	-0.255	0.193	6.29

The parameters from the potentiodynamic polarization curves are tabulated in Table 4. The i_{crit1} values did not exhibit any change with the change with hydrogen treatment temperature and time. Although there was no significant change in the magnitude of i_{crit2}, it increased with treatment temperature and time (from 4.36 mA/cm^2 to 6.98 mA/cm^2, Table 4). Rao *et al* [11] noticed similar behavior of carbon-alloyed iron aluminides in 0.5 N H_2SO_4 solution where i_{crit2} increased with increase in hydrogen charging time.

Table 4. Passivation parameters from the potentiodynamic polarization curves of the hydrogen treated samples in 0.5 N H_2SO_4 solution

Sample		ZCP	E_{pp1}	E_{pp2}	E_{cp}	E_b	E_b-E_{cp}	i_{crit1}	i_{crit2}	i_{pass}	$i_{0_{H^+/H_2}}$
Temp. (^oC)	Time (h)	mV						mA/cm^2			
Without treatment		-535	-370	-65.6	501	1480	979	18.20	4.36	0.132	$2.95X10^{-2}$
700	10	-535	-382	-75.9	516	1470	954	21.85	5.37	0.108	$3.09X10^{-2}$
700	48	-542	-391	-66.6	485	1480	995	21.37	5.24	0.137	$3.55X10^{-2}$
900	144	-535	-385	-92.2	435	1490	1055	23.89	5.99	0.162	$4.98X10^{-2}$
900	144	-542	-385	-92.5	436	1490	1054	23.91	5.81	0.191	$5.11X10^{-2}$
900	336	-535	-390	-72.3	441	1520	1079	26.12	6.34	0.434	$5.75X10^{-2}$
900	720	-546	-321	-43.4	432	1550	1118	20.87	6.98	0.767	$6.15X10^{-2}$

In the present study, the secondary anodic peak may be attributed to the oxidation of hydrogen atom formed during the initial cathodic polarization of the sample during the potentiodynamic polarization scan. The cathodic part of the potentiodynamic polarization curves (Figure 3) indicate a higher rate of hydrogen reduction on the surface of the samples, with increasing treatment temperature and time. Therefore, the i_{crit} for the secondary anodic peak also increases with increase in treatment temperature and time. The hydrogen dissolved during the high temperature treatment did not play any role on the secondary anodic peak.

The ZCP, E_{pp1}, and E_{pp2} values of the hydrogen treated samples polarized in 0.5 N H_2SO_4 (Table 4) were similar to the values of as-received samples polarized in 0.1 N to 1.0 N H_2SO_4 (Table 2). However, E_{cp} decreased whereas E_{tp} values showed a gradual increase with increase in hydrogen treatment time and temperature. Therefore, the passive ranges in the hydrogen treated Fe-16.2Al-0.54C samples increased with increasing treatment temperature and time. The i_{pass} also increased significantly with increasing treatment temperature and time. The increases in the passive range and i_{pass} must be related to the nature of the passive film that forms on the surface during polarization. In order to understand this, the effect of surface state on polarization behavior was first determined.

Effect of surface roughness

One possible reason for the change in passive film nature could be the surface condition of the hydrogen-treated samples. It is well known that passive films formed on smooth polished surfaces are superior compared to those on rough surfaces [15]. Microstructural study of the hydrogen treated samples indicated surface roughening with increasing treatment time and temperature [14].

In order to understand the effect of surface roughness, potentiodynamic polarization experiments were carried out on the as-received samples for a mirror polished surface (after cloth polishing using 1 μm alumina powder) and for a rough surface (after wheel grinding). Figure 4 shows the potentiodynamic polarization curves for both these surface finishes in 0.5 N H_2SO_4 solution. The kinetic (i.e., i_{corr}, Tafel slopes β_c and β_a) and the passivation (ZCP, E_{pp1}, E_{pp2}, E_{cp}, E_b, E_b- E_{cp}, i_{crit1}, i_{crit2}, i_{pass} and $i_{0_{H^+/H_2}}$) parameters were determined from the potentiodynamic polarization curves and are tabulated in Tables 5 and 6, respectively. Interestingly, the passivation ranges of the samples with different degree of surface roughness did not differ significantly. The

passive current density apparently decreased with increasing roughness. Therefore, the increase in the passivation ranges and i_{pass} values of hydrogen treated samples with increasing treatment temperature and time can not be attributed to the surface roughness induced by the high temperature hydrogen treatment.

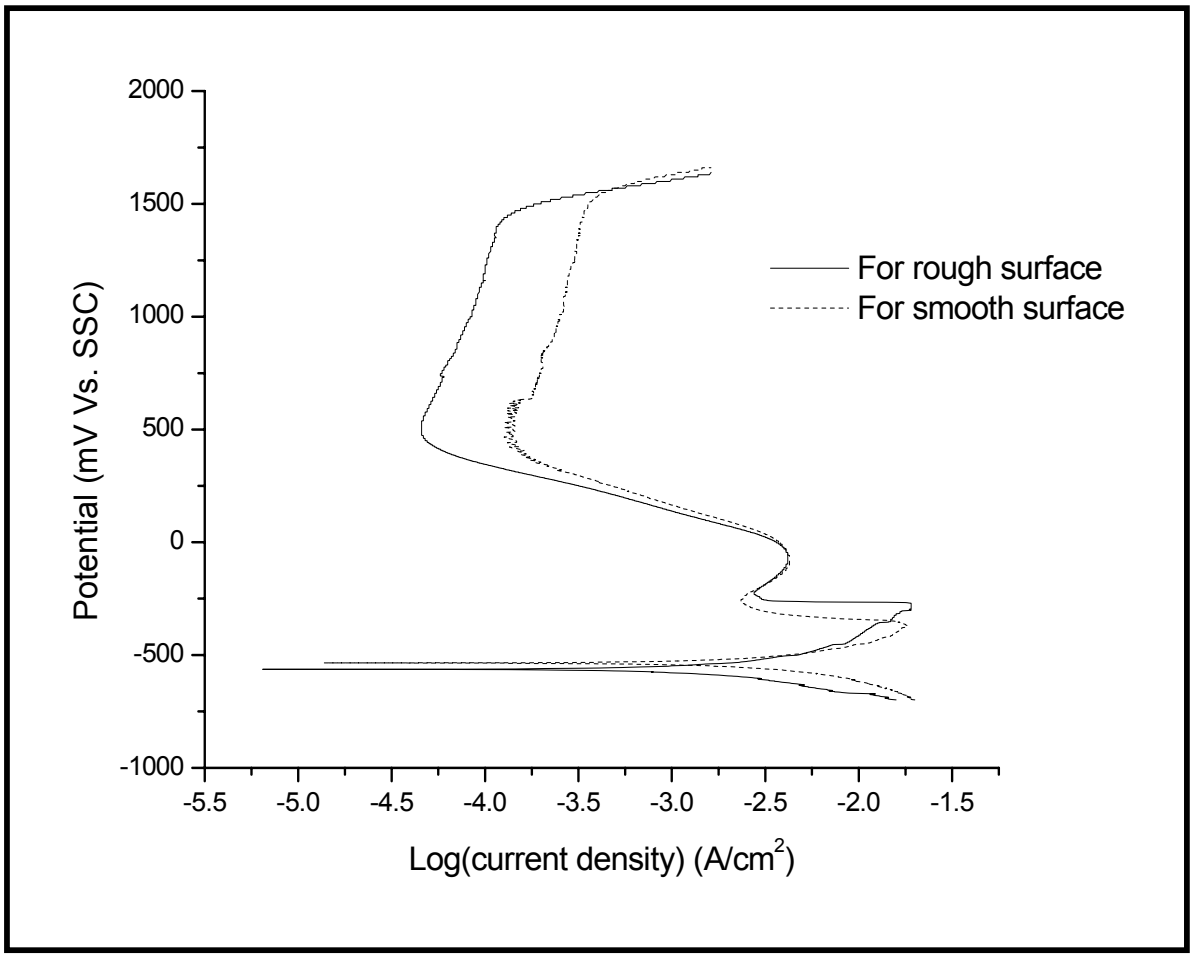

Figure 4. Potentiodynamic polarization of as-received aluminide in 0.5 N H_2SO_4 after different surface finishes

Table 5. The β_a, β_c and i_{corr} values obtained from the potentiodynamic polarization curves of as-received aluminide in 0.5 N H_2SO_4 solution for two different surface finishes.

Type of surfaces	β_c (V/decade)	β_a (V/decade)	i_{corr} (mA/cm^2)
Rough	-0.242	295	4.01
smooth	-0.252	288	4.19

Table 6. Passivation parameters obtained from the potentiodynamic polarization curves of as-received aluminide in 0.5 N H_2SO_4 solution for two different surface finishes.

H_2SO_4	ZCP	E_{pp1}	E_{pp2}	E_{cp}	E_b	E_b-E_{cp}	i_{crit1}	i_{crit2}	i_{pass}	$i_{0_{H^+/H_2}}$
N	mV						mA/cm^2			
Rough	-569	-285	-72.3	491	1420	929	19.05	4.17	0.05	$3.03X10^{-2}$
Smooth	-514	-373	-67.6	501	1470	969	18.41	4.23	0.13	$2.81X10^{-2}$

Microhardness characterization

As surface finish was discounted as the reason for the observed increase in passive current density with hydrogen treatment, it was decided to explore the possibility of changes in surface compositions, which may have caused the observed differences. Compositional changes was studied by microhardness measurements. As compositional changes result in changes in mechanical behavior, microhardness measurements can indirectly indicate surface compositional changes. A major advantage of microhardness measurements is that a large sample area can be sampled so as to obtain statistically meaningful results for comparison purposes. Further, the instrumentation involved is not sophisticated and data collection times are relatively short.

The microhardness of the bulky carbides and grains were measured in the as-received alloy as well as all the hydrogen treated samples. Hardness measurement of needle-shaped carbides was not possible because proper indentations could not be made on these small sized carbides. Moreover, they dissolved fairly early into the matrix during high temperature hydrogen treatment. A 50-gram load was applied for the measurement of hardness as this provided optimum size of the indentation. If the size of the indentation is too small, then the measurement error of the diagonal will be high. On the other hand, if a higher load is applied in order to make the indentation, the indentation mark could overlap some nearby phase. Tables 7 and 8 report microhardness results for the bulky carbides and matrix, respectively, as a function of hydrogen treatment properties.

Table 7. Hardness of bulky carbides after different high temperature hydrogen treatments.

Treatment Temp (^{o}C)	Time (h)	Diagonal (μm)	SD	FOV	%Error, +-	Hardness kg/mm^2
Without treatment		13.230	0.586	30	1.618	529.73
700	10	13.241	0.413	30	1.144	528.85
700	48	13.501	0.389	30	1.101	508.68
900	144	13.629	0.547	30	1.568	499.17
900	144	13.593	0.453	30	1.301	501.81
900	336	13.823	0.631	30	1.721	485.25
900	720	13.937	0.336	30	0.978	474.89

It is observed from Table 7 that the carbides in the sample, which was treated at 900^{o}C for 720 hours, exhibited the lowest hardness. Two duplicate samples treated at 900^{o}C for 144 h exhibited almost similar hardness. The carbides in the sample treated at 700^{o}C were not significantly affected by the hydrogen treatment. Generally, the hardness of the carbides decreased with increasing temperature and time of hydrogen treatment. The change in hardness of the carbide must be due to interaction with hydrogen and oxygen at high temperature. Hydrogen interaction with carbide results in depletion of carbon from the carbides while oxygen interaction with carbide depletes Al. Therefore, the change in carbide composition with hydrogen treatment was indirectly confirmed by microhardness measurements. The hardness of the matrix (Table 8) also decreased with increasing

hydrogen treatment time and temperature. However, the rate of decrease of hardness with increasing treatment temperature and time was lower compared to the carbides. The decrease in hardness of the matrix could probably be due to dealloying from matrix.

Table 8. Hardness of matrix after different high temperature hydrogen treatments.

Treatment		Diagonal (μm)	SD	FOV	%Error, +-	Hardness kg/mm^2
Temp (^{o}C)	Time (h)					
Without treatment		17.127	0.556	30	1.185	316.10
700	10	17.231	0.491	30	1.045	312.29
700	48	17.397	0.608	30	1.306	306.36
900	144	17.503	0.544	30	1.396	302.66
900	144	17.487	0.631	30	1.982	303.21
900	336	17.763	0.313	30	0.783	293.86
900	720	17.891	0.365	30	0.820	289.67

The lower matrix and carbide hardness with increasing temperature and time of hydrogen treatment verified surface compositional changes. As passivation of surfaces in electrolytic solutions is sensitive to surface composition, the change in passive current density with hydrogen treatment can be concluded to result from compositional changes on surfaces that occurred during the high temperature hydrogen treatment.

4. Conclusions

The salient conclusions of the present study were:

1. Electrochemical polarization studies were conducted on a carbon-alloyed iron aluminide of composition Fe-16.2Al-0.54C (in wt %) both before and after high temperature hydrogen treatments.
2. The as-received alloy, as well as the hydrogen treated samples, exhibited active-passive behavior in 0.5N H_2SO_4 acidic solution. A secondary anodic peak was observed in the polarization curves.
3. The potentiodynamic polarization behaviour of as-received alloy was studied in sulfuric acid of different normalities (0.1N to 1.0N). The corrosion rate and exchange current density for

hydrogen evolution reaction increased systematically with increasing normality of H_2SO_4, while the Tafel slopes were similar. The increased corrosion rate has been attributed to the increasing hydrogen ion concentration in the solution and to increasing exchange current density. The critical current density for the second anodic peak increased with normality due to the larger amount of hydrogen available for oxidation in solutions of higher normalities. The passive current density also increased with increasing normality.

4. The corrosion rates of the hydrogen-treated sample were similar in 0.5M H_2SO_4. The secondary anodic peak increased with increase in treatment temperature and time. This has been attributed to the evolution of hydrogen on the surface during the initial cathodic run of the potentiodynamic polarization scan. The hydrogen dissolved in the material during the high temperature hydrogen treatment did not play any role on the secondary anodic peak.
5. The increase in the passivation ranges and passive current densities of the hydrogen treated samples with increasing treatment temperature and time could not be attributed to the surface roughness induced by the high temperature hydrogen treatment. This has been related to the surface compositional changes that occurred during high temperature hydrogen treatment, which was confirmed by surface microhardness measurements.

Acknowledgement

The authors would like to acknowledge the support of Defence Research and Development Organization, Ministry of Defence, India.

References

1. C.T. Liu, K.S. Kumar, *J. Metals*, 45, pp38- , 1993.
2. 'Fracture of Fe $_3$ Al', W.R. Kerr, *Metall. Trans,* A,17, pp2298-2300, 1986.
3. 'Effect of carbon addition on structure and mechanical properties of electroslag remelted Fe–20 wt.% Al alloy', R.G. Baligidad, U. Prakash, A. Radhakrishna, *Mater. Sci. Engg.* A, 249, pp97-102 1998.
4. 'Effect of carbon content mechanical properties of electroslag remelted Fe $_3$ Al based intermetalic alloys', R.G. Baligidad, U. Prakash, V.R. Rao, P.K. Rao and N. B. ballal, *ISIJ International*, 36, pp1453-1458, 1996 .

5. 'Thermal stability and elevated temperature mechanical properties of electroslag remelted Fe-16wt.%Al-(0.14-0.5)wt.%C intermetallic alloys', U. Prakash, A. Radhakrishna and R.G. Baligidad, *Mater. Sci. Engg*, A, 230, pp188-193, 1997.
6. 'Hydrogen trapping at carbide-matrix interfaces in Fe_3Al-C intermetallics', M. Sen and R. Balasubramaniam, *Scripta Mater,* 44, pp619-623, 2001.
7. 'Effect of Al content on oxidation behaviour of ternary Fe–Al–C alloys', V.S. Rao, R.G. Baligidad and V.S. Raja, *Intermetallics*, 10, pp73-84, 2002.
8. 'On elevated temperature stability of high carbon Fe-Al alloys', R.G. Baligidad, U. Prakash and A. Radha Krishna, *Mater. Sci. Engg*, A, 265, pp301-305, 1999.
9. 'Hot corrosion of Fe $_3$ Al', D. Das, R. Balasubramaniam and M.N. Mungole, *J. Mater. Sci*, 37, pp1135-1142, 2002.
10. 'Hot corrosion of carbon alloyed Fe_3Al-based iron aluminides', D. Das, R. Balasubramaniam and M.N. Mungole*, Mater. Sci. Engg*, A*,* 338, pp24-32, 2002.
11. **'**Effect of carbon on corrosion behaviour of Fe_3Al intermetallics in 0.5 N sulphuric acid'**,** V.S. Rao, R.G. Baligidad and V.S. Raja, *Corrosion Sci*, 44, pp521-533, 2002.
12. 'A combined electrochemical and XPS study on the passivity of B2 iron aluminides in sulphuric acid solution', S. Frangini, N.B. De Cristofaro and A. Mignose, *Corrosion Sci.*, 39, pp1431-1442, 1997.
13. 'A correlation between phosphorous impurity in stainless steel and a second anodic current maximum in H_2SO_4 , A.A. Hermas, M.S. Morad and K. Ogura, *Corrosion Sci*, 41, pp2251-2266, 1999.
14. 'Hydrozen attack in carbon-alloyed iron aluminides-microstructural evolution', T. Laha, R. Balasubramaniam, A. Tewari, M.N. Mungole and R.G. Baligidad, *to be published.*
15. 'Principles and Prevention of Corrosion', D.A. Jones, Maxell Macmillan International, New York, 1992.